NeuroRegulation

ISNR INTERNATIONAL SOCIETY FOR NEUROREGULATION & RESEARCH

Neural Network Improvements Induced by REST Flotation in Chronic Lower Back Pain Patients: An Exploratory Investigation

Tyler A. McGaughey[*]*, Mary K. Gregg, and Victor S. Finomore*

West Virginia University School of Medicine, Morgantown, West Virginia, USA

Abstract

Thalamocortical dysrhythmia is a shared hallmark of numerous neurodivergent conditions. Restricted environment stimulation therapy (REST) flotation causes desirable neural shifts in anxious or depressed populations towards classically defined healthy spectra. In this exploratory investigation, chronic lower back pain patients were randomly assigned to the experimental condition, six 1-hr REST flotation sessions, or the control condition, six 1-hr nap pod sessions. Participants underwent quantitative electroencephalograms (qEEG) before and after their six sessions. Chronic lower back pain patients were chosen because of the high prevalence of the disease condition and the known network changes that contribute to the transition of pain from acute to chronic. Results showed traditional qEEG pain-associated signatures shift to reflect more regulated, healthy activity across the pain and default mode networks in our experimental condition. Dysregulation in neural oscillations can be indicative of symptomology, and the changes observed in the experimental group reflect healthier activity in all frequency bands, while the control group showed no significant changes in any 1 Hz bin. These significant cross-spectral improvements show promise for REST flotation as a supplemental nonpharmacological treatment for chronic pain.

Keywords: qEEG; chronic lower back pain; REST flotation; neural networks; default mode network

Citation: McGaughey, T. A., Gregg, M. K., & Finomore, V. S. (2023). Neural network improvements induced by REST flotation in chronic lower back pain patients: An exploratory investigation. *NeuroRegulation, 10*(2), 118–133. https://doi.org/10.15540/nr.10.2.118

***Address correspondence to**: Tyler A. McGaughey, PhD Neuroscience, Rockefeller Neuroscience Institute, West Virginia University School of Medicine, 33 Medical Center Drive, Morgantown, WV, 26506, USA. Email: tyleramcgaughey@gmail.com

Edited by:
Rex L. Cannon, PhD, Currents, Knoxville, Tennessee, USA

Reviewed by:
Rex L. Cannon, PhD, Currents, Knoxville, Tennessee, USA
Tanya Morosoli, MSc: 1) Clínica de Neuropsicología Diagnóstica y Terapéutica, Mexico City, Mexico; 2) ECPE, Harvard T. H. Chan School of Public Health, Boston, Massachussetts, USA

Introduction

Neural network alterations are a hallmark of disease states. In particular, thalamocortical dysregulations can be observed in neurodivergent populations such as Parkinson's disease, Alzheimer's disease (AD), chronic pain, and depression (Vanneste et al., 2018). The thalamocortical dysrhythmia model suggests that disturbances arise between the cortex and thalamus, impeding the flow of information. This disruption may impact cognition, movement, and sensation since higher-level cognitive functions are driven by the interactions between the thalamus and cortex.

Chronic lower back pain (CLBP) is one of the leading causes of disability worldwide, with over 550 million cases in 2019, and has one of the highest number of years lived with disabilities ratio of any disease (Chen et al., 2022). One of the critical shifts in the "chronification" of pain is the transition of pain from the motor cortex to other centers throughout the brain, such as the prefrontal cortex. Traditional interventions rely heavily on ameliorating patients' physical pain, which fails to encapsulate patient suffering as a whole. In addition, these deficits contribute to comorbidities such as anxiety, particularly kinesiophobia, and depression (Gore et al., 2012). This is keenly reflected in the representation across the quantitative electroencephalogram (qEEG) spectra as

dysregulations in the pain network and default mode network (DMN; Alshelh et al., 2018; Kisler et al., 2020).

A noninvasive method used to explore electrical brain activity, qEEG can be used during active states (listening to cues, watching stimuli, performing cognitive tasks), and rich data can also be collected during resting states. Resting-state qEEG rhythms can be indicative of states of arousal and informative of the cognitive processing and potential pathology (Babiloni et al., 2016; Koo et al., 2017; Lee et al., 2014; Trammell et al., 2017). Spectral qEEG data can be broken down by frequency bands which further elucidate various neurological mechanisms in neural networks. Dysregulated electrical activity impacts the function of networks and can indicate pathology (Cecchetti et al., 2021; Li, Pagnotta et al., 2015). This dysregulation can manifest differently by frequency band and by location or network (Gollan et al., 2014; Moon et al., 2018).

Restricted environment stimulation therapy (REST), achieved through sensory deprivation, is seen in the literature as early as the 1950s, with an uptick in rigorous clinical investigations in the last 10 years. Not only has REST flotation shown promise in reducing anxiety and depression (Jonsson & Kjellgren, 2016), but recent work by Al Zoubi et al. (2021) shows alteration in the DMN in healthy patients (Al Zoubi et al., 2021). In brief, Al Zoubi et al. (2021) saw significant changes in the following Broadman Areas (BA) as determined by the published MRI Montreal Neuroscience Imaging Atlas coordinates; 1, 4, 13, 17, 37, and 39 (Al Zoubi et al., 2021). Since REST flotation has the ability to improve neural networks, we inferred that REST flotation might be beneficial for counteracting the network alterations that contribute to the development of chronic pain. The working theory for REST flotation is that reduced sensory input may help to reset networks and alleviate pain. Therefore, our research question asks: does REST flotation alter neural network changes in CLBP patients?

Methods

All study-related procedures were approved by the West Virginia University (WVU) Institutional Review Board (AAHRPP Accredited). This substudy is part of a larger clinical trial (NCT05260918). Participants were recruited from the WVU Center for Integrated Pain Management and were enrolled from January to December of 2022. Flyers with general study information were hung in exam rooms and distributed to patients with a primary diagnosis of back pain. Interested participants completed the intake survey via QR code through Qualtrics (Qualtrics, 2023). Research personnel reviewed questionnaire responses, and individuals who met the inclusion criteria were invited to visit WVU's Rockefeller Neuroscience Institute (RNI). In brief, inclusion criteria for the study included (a) MRI compatibility, (b) right-handedness, (c) consistent medications for at least the previous 30 days, (d) chronic back pain (as defined below), (e) 18–65 years of age, (f) naïve to mindfulness intervention, and (g) the ability to enter and exit a bathtub without assistance. After a brief tour, interested participants completed the written informed consent process, which included participants going over the consent form with a trained member of the research team, being afforded the opportunity to ask any questions they may have had, and being given time to review all study-related materials prior to signing the consent form. After informed consent was obtained, participants were assigned a unique study code, which was then used to identify all study-related materials. Participants were then randomly assigned to the experimental REST flotation group or the control nap pod group. There was limited access to the master study index, which is the only index linking participants with their study code.

A total of 16 participants were enrolled, and after performing manual and statistical artificing, 10 participants' records were included in the final analyses. An additional participant was then excluded after self-reported extreme life stressors required psychiatric intervention. Therefore, the subsequent analyses are based on $N = 9$. General participant demographics are noted in Table 1.

Inclusion criteria required patients to have CLBP, defined as consistent musculoskeletal back pain that has a moderate-to-severe impact on the patient's life for at least the last 12 weeks. Participant medications are noted below, psychiatric and allergy medications were most prevalent [Supplement 1]. Medication effects were mitigated by using the Laplacian montage in all qEEG analyses.

Float Tank

REST is often achieved through the use of sensory deprivation tanks. For this investigation, we used two Deluxe Quest Floatation Suite tanks (Superior Float Tanks, n.d.). Each tank measures 238 cm in length by 198 cm in width by 224 cm in height and contains approximately 3800 L salt water with 680 kg of Epsom salt dissolved in 37° C water yielding a specific gravity of 1.30 kg/m^3.

Table 1
Participant Demographics by Group

	Mean Age (Years)	Mean Weight (Kg)	Height (cm)	M/F	Caucasian	African American	Asian
Float	39.5 ± 13.9	80.1 ± 18.3	174 ± 13.8	2/4	67%	11.5%	11.5%
Nap	26 ± 2	104.5 ± 15.9	177.8 ± 13.2	2/1	100%	0%	0%

The float tanks are thoroughly insulated to prevent light and sound pollution. Participants engaged in six biweekly float sessions, with each session lasting 1 hr and, though encouraged to float with the tank lights and music off, they were given the option to activate them at any time from inside the tanks for comfort. Participants also had the ability to signal research staff via intercom or push-button if required.

Nap Pod

The control condition for this investigation was the MetroNaps EnergyPod nap pod (MetroNaps, n.d.). Participants in this condition engaged in a similar number of sessions as the float condition. The nap pod is located in a dark, quiet room without windows. There was a motion-activated dim red light for participant safety if they needed to exit the pod for any reason. Participants also had the ability to signal research staff via intercom or push-button if required.

qEEG Recording

The qEEG was recorded using the CGX Quick-20m, an FDA-cleared wireless headset (Cognionics, n.d.). The system uses dry electrodes recorded from 19 scalp locations consistent with the International 10–20 system (FP1, FP2, F3, F4, Fz, F7, F8, C3, C4, T3, T4, T5, T6, P3, P4, Pz, O1, and O2) and references A1 and A2 (linked-ear montage). The Fp1 and Fp2 electrodes were placed carefully approximately 1 cm above the eyebrows, in line with the participant's pupils. The remaining electrodes were then stretched over the scalp. The cap is designed to reliably align with most head shapes and sizes while maintaining the integrity of the standard 10–20 system. qEEG data were collected in an awake resting state, eyes-closed condition at baseline, and again following treatment.

The qEEG was digitally recorded at 500 samples per second using NeuroGuide software (Version 3.2.7; Applied Neuroscience Inc., n.d.). A 1-Hz high-pass and 40-Hz low-pass filter were applied along with a 60-Hz notch filter to mitigate electrical artifacts. Artifact removal was performed using the NeuroGuide artifact rejection toolbox. Data was then remontaged to Laplacian and visually examined for any further artifacts (EMG, eye movement, electrode pop), which were removed manually. Though Laplacian helps to mitigate the effects of medicine as it sets the global field effects to zero, the impact on the qEEG cannot be entirely ruled out. A list of pharmaceuticals the participants took is listed in S1. Records containing at least 60 s of artifact-free data were included in the analyses. Each maintained a split-half reliability of 0.95 or higher or a test–retest value of 0.93 or higher. Finally, the records were analyzed using NeuroGuide's NaviStat software package for group comparisons using both absolute power and *z*-scored normative comparisons. The NeuroGuide Lifespan database is comprised of 727 normal individuals aged 2–82 years (Thatcher, 2008). Participants were screened prior to inclusion. Those with any history of abnormal prenatal, perinatal, or postnatal development, history of central nervous system diseases, disorders of consciousness, febrile or psychogenic convulsions, and any abnormal deviation in mental or physical development were excluded.

While EEG is recognized for temporal resolution, it lacks the spatial capabilities of other neuroimaging techniques. However, advancements have been made in source localization in EEG over the past 2 decades. Palmero-Soler improved upon the previously used sLORETA method that uses a spherical model of 6200 MRI voxels. This improvement, swLORETA or weighted sLORETA, uses a realistic head model with the boundary element method (BEM) to analyze 12,700 5-mm voxels of current source density allowing for improved source localization of subcortical structures. The centermost voxel of the BA is used to define the region of interest (ROI; Palmero-Soler et al., 2007).

NeuroGuide's NaviStat software includes groups of BAs to correlate with functional networks. Based on Navistat's definition, the pain network is defined as the somatosensory network with the inclusion of several key pain ROIs like the thalamus, amygdala,

and habenula (BA 1, 2, 3, 4, 5, 13a, 24, 32, 33, Thalamus, Habenula, and the Amygdala). Navistat defines the Default Mode Network as BA 2, 7, 10, 11, 19, 29, 30, 31, 35, 39, 40, Cerebellum Crus 1, Cerebellum Crus 2, and Cerebellum 9. See S4 (Pain) and S5 (DMN) for the Talairach coordinates of the centermost voxel of each BA ROI in the networks of interest. A paired *t*-test was used to observe changes between baseline and post-float session interventions using absolute power and *z*-scored comparison.

Statistical Analysis

Group level differences were calculated via paired *t*-test by network-defined ROIs across the frequency spectra using NeuroNavigator's NaviStat default statical package. Each *t*-test was informed by the power of the centermost voxel in each ROI according to the schema that follows. For each ROI, there were three *t*-tests (Experimental Baseline vs. Experimental Follow-Up, Control Baseline vs. Control Follow-Up, and Control Baseline vs. Experimental Baseline). However, there were only two overlapping *t*-tests with the same data input (Baseline Control vs. Baseline Experimental and Baseline vs. Follow). Therefore, a Bonferroni correction was used to correct for multiple comparisons. An initial alpha value of 0.90 was selected since these data are preliminary results based on a small sample size. After the Bonferroni correction, a *p*-value of .05 for each ROI indicates statistical significance. There is no need to correct for multiple comparisons across ROIs since each ROI has a unique set of data.

Results

Differences Between Groups

There are no significant differences between the nap and float groups at baseline via an independent two-tailed *t*-test. A paired samples *t*-test showed significant changes in the pain network in the REST flotation experimental group over time in all but six 1-Hz frequency bins out of the 30 Hz analyzed. No significant differences were observed in the nap control group paired sample *t*-test over time. An example showing significance observed in the pain network at 21 Hz in the REST floatation group (Figure 1) compared to the control group (Figure 2) is shown below. In Figure 1, there are 12 significant changes in the pain network over time for the experimental group, with no significant improvements in the control group. It is also important to note that these surface renderings represent a 1-Hz bin. Figure 5 shows the total number of significant changes across the network of interest, and the significant changes by exact ROI by hertz are shown in the supplement.

Figure 1. *Group Level Surface Rendering of 21 Hz of Significant Changes Across the Pain Network in the Float Condition.*

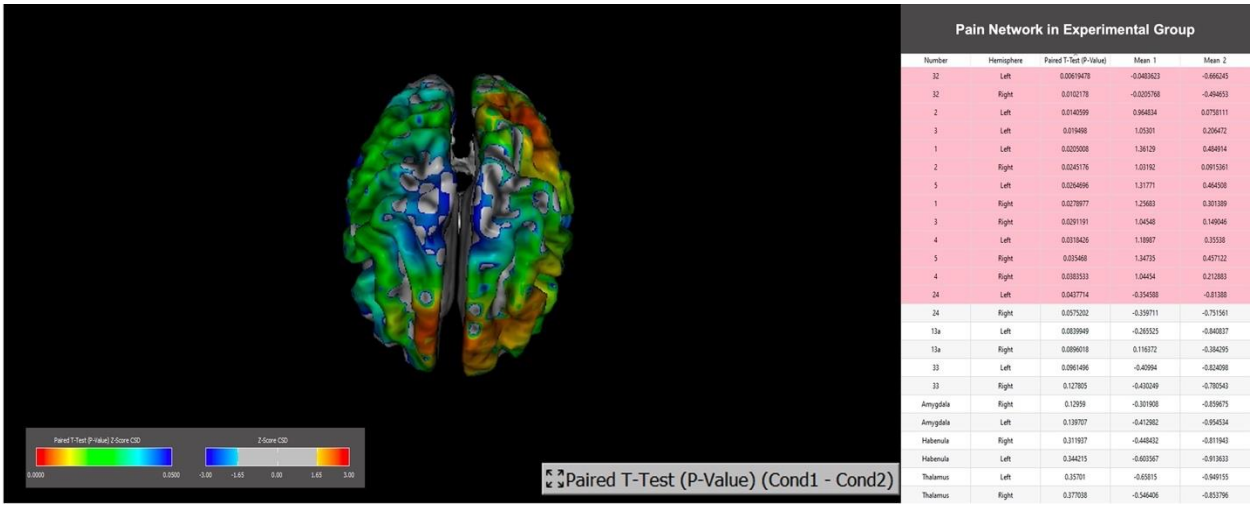

Note. Highlighted regions in the chart represent statically significant changes.

Figure 2. *Group Level Surface Rendering of 21 Hz of Significant of Significant Changes Across the Pain Network in the Control Condition.*

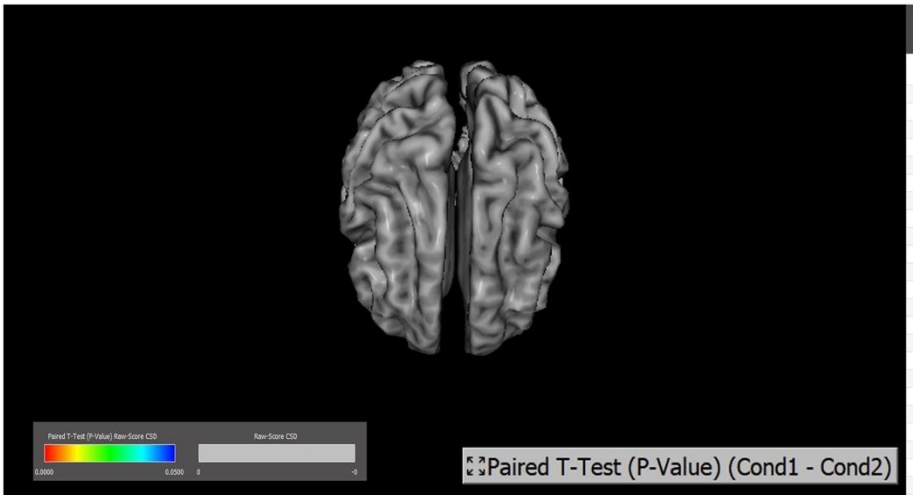

Pain Network in Control Group

Number	Hemisphere	Paired T-Test (P-Value)	Mean 1	Mean 2
1	Left	0.357104	1.22859	0.922162
1	Right	0.29295	1.25787	0.941373
13a	Left	0.451261	-0.317539	-0.43459
13a	Right	0.686714	-0.434703	-0.365246
2	Left	0.310851	0.715996	0.47853
2	Right	0.25367	0.990752	0.700352
24	Left	0.239883	-0.253391	-0.0877079
24	Right	0.263387	-0.331521	-0.0871223
3	Left	0.338147	0.94969	0.688831
3	Right	0.296423	1.12477	0.844976
32	Left	0.310023	-0.0686319	-0.042557
32	Right	0.314853	-0.256732	-0.0829705
33	Left	0.232084	-0.256507	-0.0745008
33	Right	0.255565	-0.326801	-0.061626
4	Left	0.305097	1.17809	0.901643
4	Right	0.369709	1.22844	1.00504
Thalamus	Left	0.822361	-0.267783	-0.304792
Thalamus	Right	0.883945	-0.277589	-0.250663
5	Left	0.309333	1.31863	1.02229
5	Right	0.28565	1.43917	1.1126
Habenula	Left	0.633481	-0.0256242	-0.131484
Habenula	Right	0.693874	-0.0543672	-0.144479
Amygdala	Left	0.76502	-0.262365	-0.341453
Amygdala	Right	0.997236	-0.469476	-0.468506

The same method was used to observe changes in the DMN in both experimental and control conditions. The paired samples *t*-test showed significant changes in the DMN in the REST floatation experimental group in all but three 1-Hz frequency bins out of the 30 Hz analyzed. Again, no significant changes were observed in the control group paired samples *t*-test over time. An example showing significance observed in the DMN at 4 Hz in the REST floatation group (Figure 3) compared to the control group (Figure 4) over time is shown below.

Figure 3. *Group Level Surface Rendering of Significant Changes to the DMN at 4 Hz via a Paired Samples T-Test in the Float Condition.*

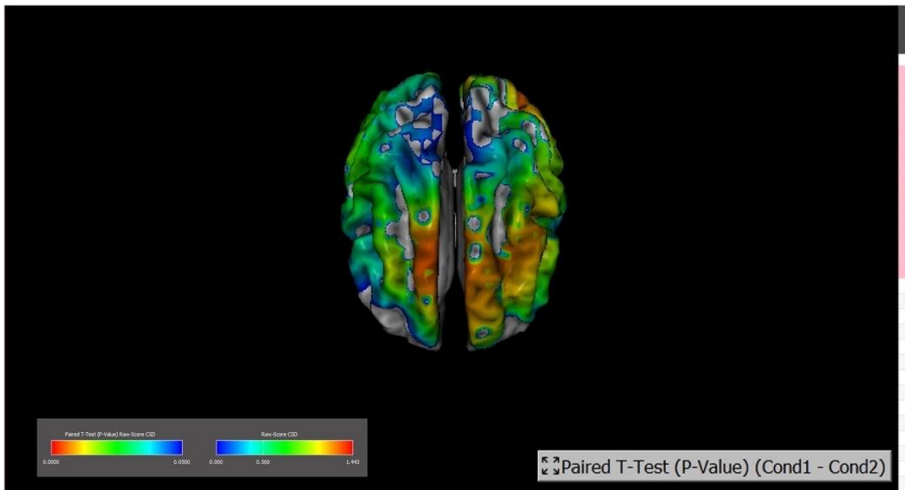

Default Mode Network in Experimental Group

Number	Hemisphere	Paired T-Test (P-Value)	Mean 1	Mean 2
7	Left	0.00656557	1.189	0.374269
40	Left	0.0111456	0.974962	0.0712733
39	Left	0.0117183	0.900198	0.00700807
2	Left	0.0140599	0.964834	0.0758111
10	Left	0.0222561	-0.0874014	-0.633314
40	Right	0.0236166	1.08459	0.11521
31	Left	0.0236704	0.549356	-0.115003
2	Right	0.0245176	1.03192	0.0915361
7	Right	0.0280681	1.15583	0.286057
19	Left	0.0305319	0.57824	-0.165881
39	Right	0.0312625	1.07401	0.130969
31	Right	0.037773	0.54697	-0.136305
10	Right	0.0419732	0.0151415	-0.474456
19	Right	0.0474049	0.799368	-0.0713547
Cerebellum_Crus1	Right	0.0643134	0.701406	-0.204936
Cerebellum_Crus2	Right	0.094722	0.481262	-0.366229
Cerebellum_Crus1	Left	0.115054	0.257546	-0.447196
Cerebellum_Crus2	Left	0.12288	0.289003	-0.380477
11	Right	0.139073	-0.361467	-0.728496
35	Left	0.140514	-0.356783	-0.931252
35	Right	0.149802	-0.283688	-0.843479
29	Right	0.163467	-0.0779028	-0.54222
Cerebellum_9	Right	0.166758	-0.0447452	-0.689977
29	Left	0.174493	-0.222314	-0.601054
Cerebellum_9	Left	0.178416	-0.12361	-0.711418
30	Right	0.211809	-0.25188	-0.742828
11	Left	0.238615	-0.595859	-0.934597
30	Left	0.251465	-0.458725	-0.866465

Note. The highlighted rows in the chart indicate statistically significant changes over time.

Figure 4. *Group Level Surface Rendering of Significant Changes to the DMN at 4 Hz via a Paired Samples T-Test in the Control Condition.*

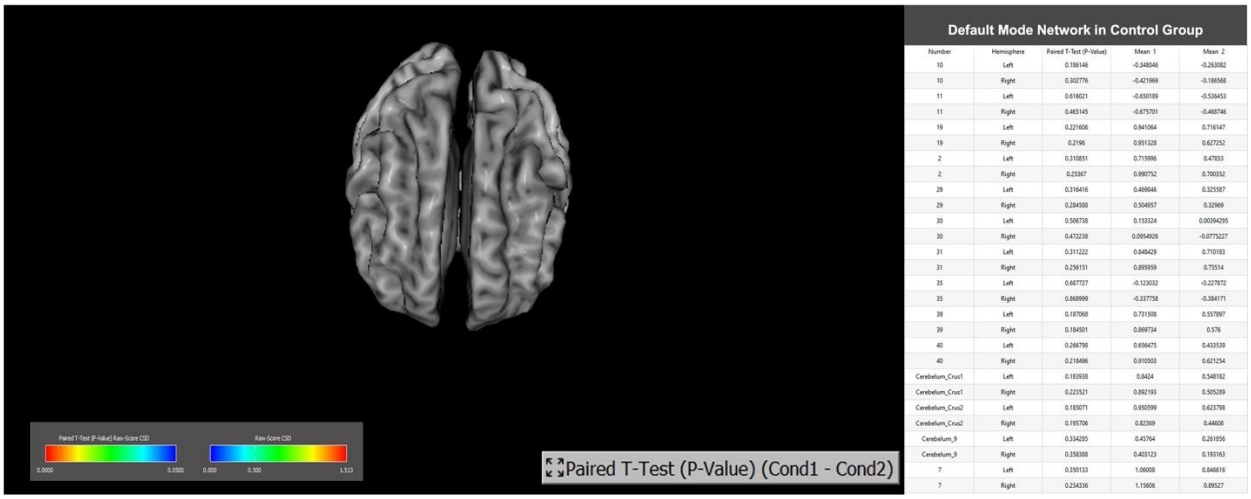

Number	Hemisphere	Paired T-Test (P-Value)	Mean 1	Mean 2
10	Left	0.186146	-0.348046	-0.263082
10	Right	0.302776	-0.421969	-0.186568
11	Left	0.616021	-0.650189	-0.536453
11	Right	0.465145	-0.675701	-0.468746
19	Left	0.221606	0.941064	0.716147
19	Right	0.2196	0.955128	0.627252
2	Left	0.310851	0.715996	0.47853
2	Right	0.25367	0.990752	0.700352
29	Left	0.316416	0.469846	0.325587
29	Right	0.284588	0.504957	0.32969
30	Left	0.506738	0.153324	0.00394295
30	Right	0.472238	0.0954826	-0.0775227
31	Left	0.311222	0.848429	0.710183
31	Right	0.256151	0.895959	0.73514
35	Left	0.687727	-0.123032	-0.227872
35	Right	0.868999	-0.337758	-0.384171
39	Left	0.187068	0.731508	0.557897
39	Right	0.184501	0.869734	0.576
40	Left	0.266798	0.656475	0.433539
40	Right	0.218496	0.910503	0.621254
Cerebelum_Crus1	Left	0.183938	0.8424	0.548182
Cerebelum_Crus1	Right	0.223521	0.892193	0.505289
Cerebelum_Crus2	Left	0.185071	0.950599	0.623798
Cerebelum_Crus2	Right	0.195706	0.82369	0.44608
Cerebelum_9	Left	0.334285	0.45764	0.261856
Cerebelum_9	Right	0.358388	0.403123	0.193163
7	Left	0.350133	1.06008	0.846616
7	Right	0.234336	1.15606	0.89527

No significant changes were seen in the control group over time in either network's 1-Hz frequency bins. The NaviStat surface renderings provide group changes in 1-Hz bins. Since all frequency bands (1–30 Hz) were included in the scope of this paper, the number of significant changes per ROI by 1-Hz bin were plotted (Figure 5) to display the significance observed in each frequency band. The bars represent changes in both Pain (5A) and DMN (5B) networks in the experimental group over time. For reference, the pain network is comprised of 24 ROIs, and the DMN is comprised of 28 ROIs. No significant changes were seen in the control group over time.

Figure 5. *Significant Changes by Frequency in Pain Network (A) and Default Mode Network (B) in 1-Hz Bins.*

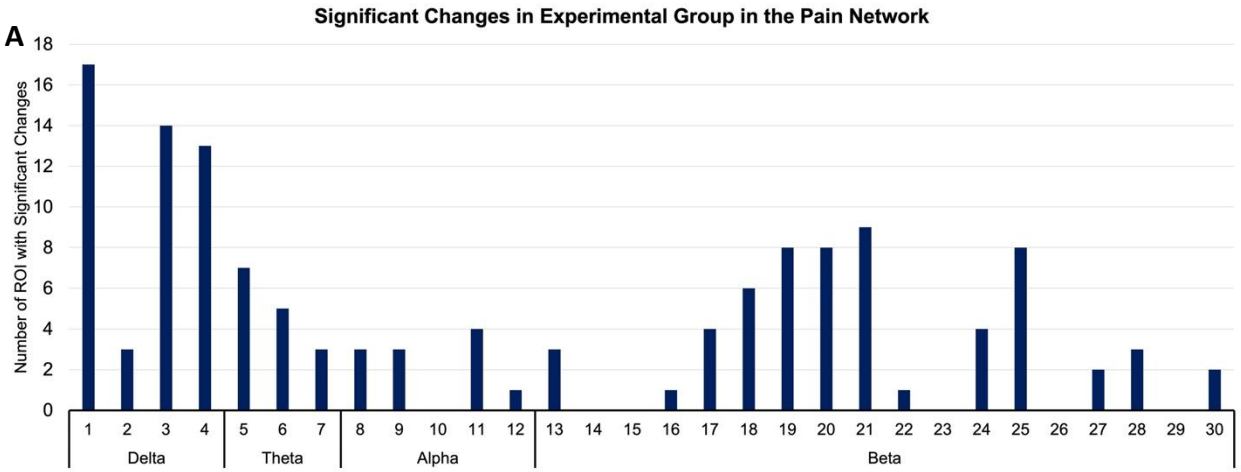

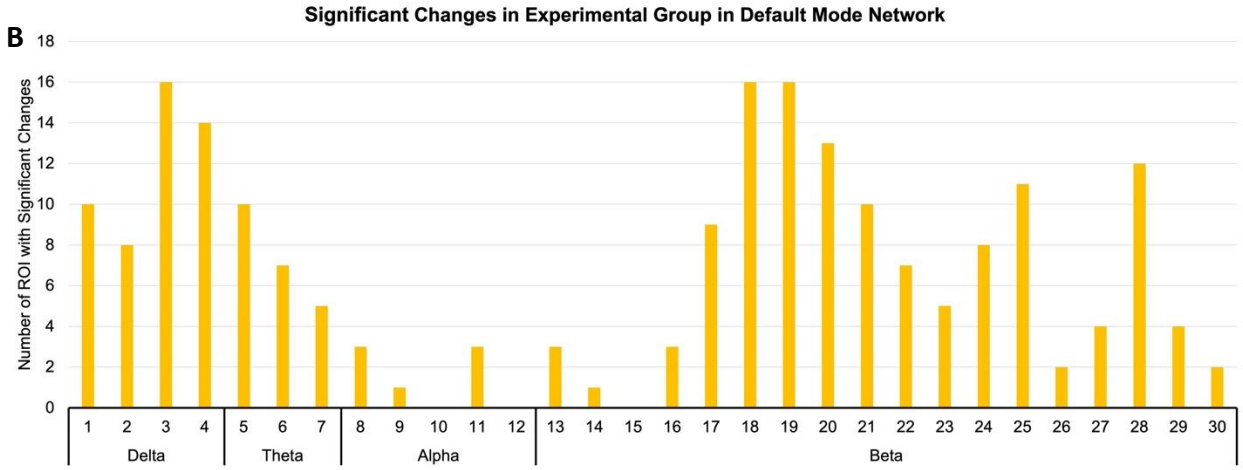

Discussion

The mechanism behind REST flotation is still unclear. REST flotation significantly reduces auditory, visual, and thermal or tactile stimulation. This reduction in stimuli may help the brain reset itself by allowing the DMN to reign supreme.

Shifts in spectral power can be indicative of functional and structural pathologies. Increases in low-frequency (2–4 Hz) and high-frequency (14–44 Hz) power in pain patients compared to healthy controls has been previously observed (Vanneste et al., 2018). Our participants displayed similar spectral data at baseline. After the float intervention, excess spectral power in all frequency bands was reduced, suggesting a healthier pattern (Supplements 2 and 3). These broad spectra significant improvements are shown in Figure 5. Significant changes were observed across all frequency bands, with the greatest spectral changes being decreases in delta (1–4 Hz), theta (4–8 Hz), and beta (17–30 Hz; Figure 1).

EEG Pain Network

The pain network is comprised of several ROIs in addition to the primary motor cortex, such as the insula, thalamus, amygdala, and habenula. While the motor cortex is responsible for the localization of pain, the interpretation and internalization of this signal take place in other regions of the brain. The thalamus is classically described as the gatekeep for inbound stimuli, while other areas like the insula, amygdala, and cingulate cortex play a central role in the "chronification" of pain (Lindsay et al., 2021).

Delta (1–4 Hz) activity is seen in deep, dreamless sleep. It has implications in pain, as Li, Ge, and colleagues (2020) found that elevated delta power is seen in increased neuropathic pain, while decreases in delta power are correlated with pain attenuation (Li, Ge, et al., 2020). Changes in delta activity at 4 Hz are represented in Figure 2 (Experimental) and Figure 3 (Control). Improvement in delta band frequencies in pain patients may help to regulate sleep and nociceptive signaling.

Theta (4–8 Hz) occurs in both sleep and wakeful states. Increased spectral theta power is seen in chronic pain (Fallon et al., 2018). Pinheiro and colleagues (2016) conducted a review and surmised that chronic pain patients display higher power in lower frequencies at rest compared to healthy individuals (Pinheiro et al., 2016).

Healthy qEEG spectra resemble a bell curve with a peak in the alpha band (Furman et al., 2020). Alpha can be viewed as a conveyer system that carries one from internal (slower frequencies) to external (faster frequencies) states of arousal. Healthy, synchronous alpha activity helps one to effectively maneuver between concentration and relaxation cycles (Sterman et al., 1994). Dysregulated alpha power can lead to interruptions in this cycle, impacting cognitive performance. Pain patient spectra tend to show dampened and slowed alpha activity, with increased power in the theta and beta bands. Other known disease states with cognitive impairment as their hallmark tend to present with a similar alpha/theta pattern (Özbek et al., 2021). Some researchers suggest that slower alpha may indicate increased sensitivity to pain (Furman et al., 2020). In this study, we observed a rightward shift in alpha band activity toward a healthier spectral presentation. Theta/alpha dysregulation is a hallmark of thalamocortical dysregulation and is

especially noted in pain patients (Prichep et al., 2018). Regulation toward healthy, normal spectra may indicate movement toward symptom reduction and overall improvement in cortical activity.

The increase in the delta band is associated with internal stressors including poor pain processing, kinesiophobia, and rumination (Li, Ge, et al., 2020). An increase in the beta band amplitude is associated with external pain-stressors such as societal stressors, loss of work, and back pain associated stigmas (Teixeira et al., 2022). These processing centers are overworked and cannot effectively communicate with one other, which is necessary to resolve the issues outlined above. Essentially, these processing centers are overworking with little to show for it. Therefore, our qEEG spectral shifts translate into a more efficient conveyer and decreased workload on the processing centers, translating to a significantly more efficient system (Zolezzi et al., 2023). Ergo, the experimental group is showing fewer disease-related qEEG signatures, such as thalamocortical dysrhythmias, which may translate to an improved quality of life.

Increased high beta activity has been observed in the chronic pain population. Excess high-beta power can lead to psychological discomfort and feelings of stress or anxiety (Díaz et al., 2019). Reducing the increase in beta power is often a target for neurofeedback interventions aiming to improve both chronic pain symptoms and pain-related comorbidities (Hassan et al., 2015; Vučković et al., 2019; Wang et al., 2019). Regulation of the beta band serves to improve symptoms of pain and anxiety alike.

EEG in Default Mode Network

Numerous recent works have shown alterations in the DMN in chronic pain states (Alshelh et al., 2018; Loggia et al., 2013). The DMN is classically discussed as the network invoked when there is a light cognitive load. However, the DMN plays a key function in many self-awareness and introspective tasks. The DMN is a relatively young evolutionary by-product because of the required advancements in cortex development and focus on internal stimuli instead of extrinsic rewards (Smallwood et al., 2021). The DMN also has close ties to the somatosensory and motor cortices. Therefore, it is not a far stretch of the imagination that the literature has shown a connection between the decrease in DMN activity and increased pain rumination (Kucyi et al., 2014). In addition, alterations to the DMN contribute to neural deficits associated with cognitive impairment in many disease states like AD, depression, ADHD, and Parkinson's disease (Mohan et al., 2016).

The DMN is comprised of the precuneus, posterior cingulate, medial prefrontal cortex, and bilateral temporoparietal junction (BA 2, 7, 10, 11, 19, 29, 30, 31, 35, 39, 40). The DMN is one of the most widely studied resting-state neural networks. This network is considered to oppose the central executive network as it is dominant in resting states when the brain is not actively involved in a task and, conversely, becomes deactivated during externally oriented cognitive processing.

Delta frequencies are imperative for memory formation, especially in the DMN (Neuner et al., 2014). Delta also plays a role in cognitive processing, with increases in power being observed during cognitive tasks (Harmony, 2013). In clinical populations, dysregulation in delta power and connectivity is observed in the DMN and is believed to be the underpinnings of psychopathology (Baenninger et al., 2017). Regulation in delta frequency power could be helpful in cognitive flexibility, sleep, and memory. Delta frequencies are highly correlated with DMN activity and the Para-hippocampal gyrus, and it is believed that this link in the delta frequencies is imperative for memory (Neuner et al., 2014).

Like delta, theta power increases during cognitive load (Diaz-Piedra et al., 2020). Frontal theta power is observed during mental processing and is negatively correlated with DMN activity. The inability to regulate frontal midline theta power can inhibit DMN activation (Scheeringa et al., 2008). Increased widespread slow-wave activity (delta and theta) in the DMN is a biomarker for AD (White et al., 2013).

Alpha, the brain's idling rhythm, is the predominant rhythm of the DMN. Alpha activity in the DMN is dominant when internal processing occurs, such as self-referential thinking and has implications in memory (Klimesch et al., 2008; Knyazev et al., 2011). The alpha oscillations help to keep the brain disengaged from external stimuli whilst engaging in introspection during resting state (Foxe & Snyder, 2011). Alpha band dysregulation in the DMN is observed in neuropsychiatric disorders such as AD, schizophrenia, and posttraumatic stress disorder (PTSD; Jafari et al., 2020; Tu et al., 2020). Decreased alpha power is thought to be the underpinning of hypervigilance in PTSD populations. Alpha band activity is believed to be imperative for information sharing in the DMN and, therefore,

regulation of this band is vital for the overall health of the network.

Beta activity in the posterior cingulate is observed in cross-network interaction and functional integration of information (de Pasquale et al., 2012). This frequency band in resting states is believed to be one of the mechanisms used in the predictive coding of stimuli (Betti et al., 2021). Engel and Fries argue that beta rhythms maintain brain states, and alterations in beta activity are representative of detriments in cognition (Engel & Fries, 2010).

Clinical Impact

Each frequency band impacts the function and connection between hubs within networks. Alterations in oscillations can impact cognition, sensation, movement, perception, and behavior. The health of the DMN affects the health and behavior of the entire brain. In this study, REST flotation shifts qEEG to reflect healthier spectral power in two key pain networks, the DMN and pain network. Initially, our population varied from healthy, pain-free spectra. Typically, normal pain-free spectra clearly display a peak in the alpha frequency band; however, thalamocortical dysrhythmias tend to show increases in theta and beta frequencies that reflect symptomatic pain experiences (Prichep et al., 2018). Restoration of the natural, alpha-dominant frequency may lend to the improvement of a wide array of symptoms (Kisler et al., 2020; Schuurman et al., 2023). In our experimental intervention, we see a significant decrease in beta/theta bands with a slight increase in the alpha band. While these findings are preliminary, these significant neural network changes are often seen before behavioral outcomes. Therefore, with a further longitudinal investigation, REST flotation may prove beneficial as a supplemental nonpharmacological treatment for CLBP because it improves regulation across neural networks.

Conclusion

Thalamocortical dysrhythmias are observed in many neuropsychiatric and neurodivergent populations. Dysregulated neural oscillations can manifest in various behavioral and symptomatic experiences. A CLBP population was the center of this investigation because of the abhorrent alterations caused by chronic pain and the pervasiveness of CLBP. Our overall goal was to determine what, if any, effect REST flotation may have on neural networks. If REST flotation is able to improve neural networks, then it may prove useful as a supplemental nonpharmacological treatment for CLBP. In both networks of interest, we observed significant changes towards healthy pain-free spectra in the float group, while no significant changes were seen in the controls. These improvements demonstrate the effectiveness of REST flotation in altering neural networks. Therefore, REST flotation shows promise as a supplemental intervention for CLBP.

Limitations and Future Work

There are several key limitations to note in this investigation. First, this is a pilot investigation with a relatively small number of participants. Further investigation is needed to verify these data and trends, and a greater sample size is also needed to cross-examine the effects of biological sex on pain processing. These findings could be further corroborated by incorporating more expository investigational modalities, such as functional magnetic resonance imaging, to investigate changes in deeper neural networks. Also, additional behavioral outcomes should be assessed to substantiate these findings. Results from this study could be partially due to a mild reduction in inflammation, which could be further elucidated via serum biomarkers. Lastly, more diverse pain syndromes should be investigated to determine whether these findings translate to other populations.

Acknowledgement

A special thanks to J. H. Stovall and B. Rawls for their review of this manuscript. In addition, we would like to thank J. Ramadan and J. Suffridge for their technical expertise.

Author Disclosure

The authors have no disclosures.

References

Al Zoubi, O., Misaki, M., Bodurka, J., Kuplicki, R., Wohlrab, C., Schoenhals, W. A., Refai, H. H., Khalsa, S. S., Stein, M. B., Paulus, M. P., & Feinstein, J. S. (2021). Taking the body off the mind: Decreased functional connectivity between somatomotor and default-mode networks following Floatation-REST. *Human Brain Mapping, 42*(10), 3216–3227. https://doi.org/10.1002/hbm.25429

Alshelh, Z., Marciszewski, K. K., Akhter, R., Di Pietro, F., Mills, E. P., Vickers, E. R., Peck, C. C., Murray, G. M., & Henderson, L. A. (2018). Disruption of default mode network dynamics in acute and chronic pain states. *NeuroImage: Clinical, 17*, 222–231. https://doi.org/10.1016/j.nicl.2017.10.019

Applied Neuroscience, Inc. (n.d.). NeuroGuide (Version 3.2.7) [Computer software].

Babiloni, C., Lizio, R., Marzano, N., Capotosto, P., Soricelli, A., Triggiani, A. I., Cordone, S., Gesualdo, L., & Del Percio, C. (2016). Brain neural synchronization and functional coupling in Alzheimer's disease as revealed by resting state EEG rhythms. *International Journal of Psychophysiology, 103*, 88-102. https://doi.org/10.1016/j.ijpsycho.2015.02.008

Baenninger, A., Palzes, V. A., Roach, B. J., Mathalon, D. H., Ford, J. M., & Koenig, T. (2017). Abnormal coupling between default mode network and delta and beta band brain electric activity in psychotic patients. *Brain Connectivity, 7*(1), 34–44. https://doi.org/10.1089/brain.2016.0456

Betti, V., Della Penna, S., De Pasquale, F., & Corbetta, M. (2021). Spontaneous beta band rhythms in the predictive coding of natural stimuli. *Neuroscientist, 27*(2), 184–201. https://doi.org/10.1177/1073858420928988

Cecchetti, G., Agosta, F., Basaia, S., Cividini, C., Cursi, M., Santangelo, R., Caso, C., Minicucci, F., Magnani, G., & Filippi, M. (2021). Resting-state electroencephalographic biomarkers of Alzheimer's disease. *NeuroImage: Clinical, 31*, 102711. https://doi.org/10.1016/j.nicl.2021.102711

Chen, S., Chen, M., Wu, X., Lin, S., Tao, C., Cao, H., Shao, Z., & Xiao, G. (2022). Global, regional and national burden of low back pain 1990–2019: A systematic analysis of the Global Burden of Disease study 2019. *Journal of Orthopaedic Translation, 32*, 49–58. https://doi.org/10.1016/j.jot.2021.07.005

Cognionics. (n.d.). CGX Quick-20m wireless 20-channel EEG headset. [Apparatus].

de Pasquale, F., Della Penna, S., Snyder, A. Z., Marzetti, L., Pizzella, V., Romani, G. L., & Corbetta, M. (2012). A cortical core for dynamic integration of functional networks in the resting human brain. *Neuron, 74*(4), 753–764. https://doi.org/10.1016/j.neuron.2012.03.031

Díaz, H., Cid, F. M., Otárola, J., Rojas, R., Alarcón, O., & Cañete, L. (2019). EEG Beta band frequency domain evaluation for assessing stress and anxiety in resting, eyes closed, basal conditions. *Procedia Computer Science, 162*, 974–981. https://doi.org/10.1016/j.procs.2019.12.075

Diaz-Piedra, C., Sebastián, M. V., & Di Stasi, L. L. (2020). EEG theta power activity reflects workload among army combat drivers: an experimental study. *Brain Sciences, 10*(4), 199. https://doi.org/10.3390/brainsci10040199

Engel, A. K., & Fries, P. (2010). Beta-band oscillations—signalling the status quo? *Current Opinion in Neurobiology, 20*(2), 156–165. https://doi.org/10.1016/j.conb.2010.02.015

Fallon, N., Chiu, Y., Nurmikko, T., & Stancak, A. (2018). Altered theta oscillations in resting EEG of fibromyalgia syndrome patients. *European Journal of Pain, 22*(1), 49–57. https://doi.org/10.1002/ejp.1076

Foxe, J. J., & Snyder, A. C. (2011). The role of alpha-band brain oscillations as a sensory suppression mechanism during selective attention. *Frontiers in Psychology, 2*, 154. https://doi.org/10.3389/fpsyg.2011.00154

Furman, A. J., Prokhorenko, M., Keaser, M. L., Zhang, J., Chen, S., Mazaheri, A., & Seminowicz, D. A. (2020). Sensorimotor peak alpha frequency is a reliable biomarker of prolonged pain sensitivity. *Cerebral Cortex, 30*(12), 6069–6082. https://doi.org/10.1093/cercor/bhaa124

Gollan, J. K., Hoxha, D., Chihade, D., Pflieger, M. E., Rosebrock, L., & Cacioppo, J. (2014). Frontal alpha EEG asymmetry before and after behavioral activation treatment for depression. *Biological Psychology, 99*, 198–208. https://doi.org/10.1016/j.biopsycho.2014.03.003

Gore, M., Sadosky, A., Stacey, B. R., Tai, K.-S., & Leslie, D. (2012). The burden of chronic low back pain: Clinical comorbidities, treatment patterns, and health care costs in usual care settings. *Spine, 37*(11), E668–E677. https:doi.org/10.1097/BRS.0b013e318241e5de

Harmony, T. (2013). The functional significance of delta oscillations in cognitive processing. *Frontiers in Integrative Neuroscience, 7*, 83. https://doi.org/10.3389/fnint.2013.00083

Hassan, M. A., Fraser, M., Conway, B. A., Allan, D. B., & Vuckovic, A. (2015). The mechanism of neurofeedback training for treatment of central neuropathic pain in paraplegia: A pilot study. *BMC Neurology, 15*, Article 200. https://doi.org/10.1186/s12883-015-0445-7

Jafari, Z., Kolb, B. E., & Mohajerani, M. H. (2020). Neural oscillations and brain stimulation in Alzheimer's disease. *Progress in Neurobiology, 194*, 101878. https://doi.org/10.1016/j.pneurobio.2020.101878

Jonsson, K., & Kjellgren, A. (2016). Promising effects of treatment with flotation-REST (restricted environmental stimulation technique) as an intervention for generalized anxiety disorder (GAD): A randomized controlled pilot trial. *BMC Complementary and Alternative Medicine, 16*, Article 108. https://doi.org/10.1186/s12906-016-1089-x

Kisler, L. B., Kim, J. A., Hemington, K. S., Rogachov, A., Cheng, J. C., Bosma, R. L., Osborne, N. R., Dunkley, B. T., Inman, R. D., & Davis, K. D. (2020). Abnormal alpha band power in the dynamic pain connectome is a marker of chronic pain with a neuropathic component. *NeuroImage: Clinical, 26*, 102241. https://doi.org/10.1016/j.nicl.2020.102241

Klimesch, W., Freunberger, R., Sauseng, P., & Gruber, W. (2008). A short review of slow phase synchronization and memory: Evidence for control processes in different memory systems? *Brain Research, 1235*, 31–44. https://doi.org/10.1016/j.brainres.2008.06.049

Knyazev, G. G., Slobodskoj-Plusnin, J. Y., Bocharov, A. V., & Pylkova, L. V. (2011). The default mode network and EEG alpha oscillations: An independent component analysis. *Brain Research, 1402*, 67–79. https://doi.org/10.1016/j.brainres.2011.05.052

Koo, P. C., Thome, J., Berger, C., Foley, P., & Hoeppner, J. (2017). Current source density analysis of resting state EEG in depression: A review. *Journal of Neural Transmission (Vienna), 124*(Suppl. 1), 109–118. https://doi.org/10.1007/s00702-015-1432-2

Kucyi, A., Moayedi, M., Weissman-Fogel, I., Goldberg, M. B., Freeman, B. V., Tenenbaum, H. C., & Davis, K. D. (2014). Enhanced medial prefrontal-default mode network functional connectivity in chronic pain and its association with pain rumination. *The Journal of Neuroscience, 34*(11), 3969–3975. https://doi.org/10.1523/JNEUROSCI.5055-13.2014

Lee, S.-H., Yoon, S., Kim, J.-I., Jin, S.-H., & Chung, C. K. (2014). Functional connectivity of resting state EEG and symptom severity in patients with post-traumatic stress disorder. *Progress in Neuro-Psychopharmacology and Biological Psychiatry, 51*, 51–57. https://doi.org/10.1016/j.pnpbp.2014.01.008

Li, Y.-D., Ge, J., Luo, Y.-J., Xu, W., Wang, J., Lazarus, M., Hong, Z.-Y., Qu, W.-M., & Huang, Z.-L. (2020). High cortical delta power correlates with aggravated allodynia by activating anterior cingulate cortex GABAergic neurons in neuropathic pain mice. *Pain, 161*(2), 288–299. https://doi.org/10.1097/j.pain.0000000000001725

Li, L., Pagnotta, M. F., Arakaki, X., Tran, T., Strickland, D., Harrington, M., & Zouridakis, G. (2015). *Brain activation profiles in mTBI: Evidence from combined resting-state EEG and MEG activity*. 37th Annual International Conference of the IEEE Engineering in Medicine and Biology Society (EMBC) (pp. 6963–6966) Milan, Italy https://doi.org/10.1109/EMBC.2015.7319994

Lindsay, N. M., Chen, C., Gilam, G., Mackey, S., & Scherrer, G. (2021). Brain circuits for pain and its treatment. *Science Translational Medicine, 13*(619), eabj7360. https://doi.org/10.1126/scitranslmed.abj7360

Loggia, M. L., Kim, J., Gollub, R. L., Vangel, M. G., Kirsch, I., Kong, J., Wasan, A. D., & Napadow, V. (2013). Default mode network connectivity encodes clinical pain: An arterial spin labeling study. *Pain, 154*(1), 24–33. https://doi.org/10.1016/j.pain.2012.07.029

MetroNaps. (n.d.). EnergyPod nap pod. [Apparatus]. https://metronaps.com/#energypod

Mohan, A., Roberto, A. J., Mohan, A., Lorenzo, A., Jones, K., Carney, M. J., Liogier-Weyback, L., Hwang, S., & Lapidus, K. A. (2016). The significance of the default mode network

(DMN) in neurological and neuropsychiatric disorders: A review. *Yale Journal of Biology and Medicine, 89*(1), 49–57.

Moon, S.-Y., Choi, Y. B., Jung, H. K., Lee, Y. I., & Choi, S.-H. (2018). Increased frontal gamma and posterior delta powers as potential neurophysiological correlates differentiating posttraumatic stress disorder from anxiety disorders. *Psychiatry Investigation, 15*(11), 1087–1093. https://doi.org/10.30773/pi.2018.09.30

Neuner, I., Arrubla, J., Werner, C. J., Hitz, K., Boers, F., Kawohl, W., & Shah, N. J. (2014). The default mode network and EEG regional spectral power: A simultaneous fMRI-EEG study. *PLoS ONE, 9*(2), Article e88214. https://doi.org/10.1371/journal.pone.0088214

Özbek, Y., Fide, E., & Yener, G. G. (2021). Resting-state EEG alpha/theta power ratio discriminates early-onset Alzheimer's disease from healthy controls. *Clinical Neurophysiology, 132*(9), 2019–2031. https://doi.org/10.1016/j.clinph.2021.05.012

Palmero-Soler, E., Dolan, K., Hadamschek, V., & Tass, P. A. (2007). swLORETA: A novel approach to robust source localization and synchronization tomography. *Physics in Medicine & Biology, 52*(7), 1783–1800. https://doi.org/10.1088/0031-9155/52/7/002

Pinheiro, E. S. D. S., De Queirós, F. C., Montoya, P., Santos, C. L., Do Nascimento, M. A., Ito, C. H., Silva, M., Santos, D. B. N., Benevides, S., Miranda, J. G. V., Sá, K. N., & Bapista A. F. (2016). Electroencephalographic patterns in chronic pain: A systematic review of the literature. *PLoS ONE, 11*(2), Article e0149085. https://doi.org/10.1371/journal.pone.0149085

Prichep, L. S., Shah, J., Merkin, H., & Hiesiger, E. M. (2018). Exploration of the pathophysiology of chronic pain using quantitative EEG source localization. *Clinical EEG and Neuroscience, 49*(2), 103-113. https://doi.org/10.1177/1550059417736444

Qualtrics. (2023). Online intake survey. [Software].

Scheeringa, R., Bastiaansen, M. C., Petersson, K. M., Oostenveld, R., Norris, D. G., & Hagoort, P. (2008). Frontal theta EEG activity correlates negatively with the default mode network in resting state. *International Journal of Psychophysiology, 67*(3), 242–251. https://doi.org/10.1016/j.ijpsycho.2007.05.017

Schuurman, B. B., Vossen, C. J., Van Amelsvoort, T. A. M. J., & Lousberg, R. L. (2023). Does baseline EEG activity differ in the transition to or from a chronic pain state? A longitudinal study. *Pain Practice, 23*(5), 479–492. https://doi.org/10.1111/papr.13204

Smallwood, J., Bernhardt, B. C., Leech, R., Bzdok, D., Jefferies, E., & Margulies, D. S. (2021). The default mode network in cognition: A topographical perspective. *Nature Reviews Neuroscience, 22*(8), 503–513. https://doi.org/10.1038/s41583-021-00474-4

Sterman, M. B., Mann, C. A., Kaiser, D. A., & Suyenobu, B. Y. (1994). Multiband topographic EEG analysis of a simulated visuomotor aviation task. *International Journal of Psychophysiology, 16*(1), 49–56. https://doi.org/10.1016/0167-8760(94)90041-8

Superior Float Tanks. (n.d.). Deluxe Quest Flotation Suite. [Apparatus]. https://www.superiorfloattanks.com/new-products-1/the-deluxe-quest-float-suite

Teixeira, P. E. P., Pacheco-Barrios, K., Uygur-Kucukseymen, E., Machado, R. M., Balbuena-Pareja, A., Giannoni-Luza, S., Luna-Cuadros, M. A., Cardenas-Rojas A., Gonzalez-Mego P., Mejia-Pando, P.F., Wagner, T., Dipietro., & Fregni, F. (2022). Electroencephalography signatures for conditioned pain modulation and pain perception in nonspecific chronic low back pain-an exploratory study. *Pain Medicine, 23*(3), 558–570. https://doi.org/10.1093/pm/pnab293

Thatcher, R. (2008). *NeuroGuide manual and tutorial*. St. Petersburg, FL: Applied Neuroscience.

Trammell, J. P., MacRae, P. G., Davis, G., Bergstedt, D., & Anderson, A. E. (2017). The relationship of cognitive performance and the theta-alpha power ratio is age-dependent: An EEG study of short term memory and reasoning during task and resting-state in healthy young and old adults. *Frontiers in Aging Neuroscience, 9*, 364. https://doi.org/10.3389/fnagi.2017.00364

Tu, Y., Fu, Z., Mao, C., Falahpour, M., Gollub, R. L., Park, J., Wilson, G., Napadow, V., Gerber, J., Chan, S.-T., Edwards, R. R., Kaptchuk, T. J., Liu, T., Calhoun, V., Rosen, B., & Kong, J. (2020). Distinct thalamocortical network dynamics are associated with the pathophysiology of chronic low back pain. *Nature Communications, 11*(1), Article 3948. https://doi.org/10.1038/s41467-020-17788-z

Vanneste, S., Song, J.-J., & De Ridder, D. (2018). Thalamocortical dysrhythmia detected by machine learning. *Nature Communications, 9*(1), Article 1103. https://doi.org/10.1038/s41467-018-02820-0

Vučković, A., Altaleb, M. K. H., Fraser, M., McGeady, C., & Purcell, M. (2019). EEG correlates of self-managed neurofeedback treatment of central neuropathic pain in chronic spinal cord injury. *Frontiers in Neuroscience, 13*, 762. https://doi.org/10.3389/fnins.2019.00762

Wang, S.-Y., Lin, I.-M., Fan, S.-Y., Tsai, Y.-C., Yen, C.-F., Yeh, Y.-C., Huang, M.-F., Lee, Y., Chiu, N.-M., Hung, C.-F., Wang, P.-W., Liu, T.-L., & Lin, H.-C. (2019). The effects of alpha asymmetry and high-beta down-training neurofeedback for patients with the major depressive disorder and anxiety symptoms. *Journal of Affective Disorders, 257*, 287–296. https://doi.org/10.1016/j.jad.2019.07.026

White, T. P., Jansen, M., Doege, K., Mullinger, K. J., Park, S. B., Liddle, E. B., Gowland, P. A., Francis, S. T., Bowtell, R., & Liddle, P. F. (2013). Theta power during encoding predicts subsequent-memory performance and default mode network deactivation. *Human Brain Mapping, 34*(11), 2929–2943. https://doi.org/10.1002/hbm.22114

Zolezzi, D. M., Alonso-Valerdi, L. M., & Ibarra-Zarate, D. I. (2023). EEG frequency band analysis in chronic neuropathic pain: A linear and nonlinear approach to classify pain severity. *Computer Methods and Programs in Biomedicine, 230*, 107349. https://doi.org/10.1016/j.cmpb.2023.107349

Received: April 06, 2023
Accepted: April 23, 2023
Published: June 29, 2023

Appendix

Supplemental Materials

Supplement 1
Participant Medications Verified via Chart Review

Participant	Medication	Purpose/Class
Float 1	Dexedrine 10mg PO Daily	Stimulant
	Adderall XR 30mg PO Daily	Stimulant
Float 2	Allegra 30 mg PO Daily	Allergy
	Flonase PRN	Allergy
	Naproxen 1000 mg PRN	NSAID
Float 3	Methotrexate 2.5mg PO Daily	Antimetabolites
	Enbrel 50 mg SubQ weekly	TNF Blocker
Float 4	Adderall XR 20mg BID	Stimulant
	Methocarbamol 500mg PRN	Muscle Relaxer
Float 5	No prescribed medications	
Float 6	No prescribed medications	
Nap 1	Duloxetine 20mg PO Daily	Antidepressant
Nap 2	No prescribed medications	
Nap 3	Buspar 10mg BID	Anxiolytic
	Trazadone	Antidepressant
	Colchicine 0.6mg PRN	Gout

Supplement 2:

Pain Network t-Test

		Delta			Theta			Alpha			Beta																			
ROI NAME	ROI LOCATION	1 Hz	2 Hz	3 Hz	4 Hz	5 Hz	6 Hz	7 Hz	8 Hz	9 Hz	10 Hz	11 Hz	12 Hz	13 Hz	14 Hz	15 Hz	16 Hz	17 Hz	18 Hz	19 Hz	20 Hz	21 Hz	22 Hz	23 Hz	24 Hz	25 Hz	26 Hz	27 Hz	28 Hz	29 Hz	30 Hz
1 - L	Post Central Gyrus	0.020	NS	0.034	0.021	0.044	0.016	0.041	0.034	0.033	NS	0.016	0.034	0.024	NS	NS	NS	0.040	0.023	0.039	0.041	0.045	NS	NS	NS	NS	NS	NS	NS	NS	NS
1 - R	Post Central Gyrus	NS	NS	0.018	0.028	0.043	NS	NS	NS	NS	NS	NS	NS	NS	NS	NS	NS	NS	NS	0.029	0.041	0.032	NS	NS	0.036	0.047	NS	NS	NS	NS	NS
2 - L	Post Central Gyrus	0.010	0.029	0.022	0.014	0.027	0.012	0.028	NS	NS	NS	0.029	NS	0.047	NS	NS	0.045	NS	0.035	NS	0.022	0.029	0.044	NS	NS	NS	NS	0.037	0.037	NS	0.044
2 - R	Post Central Gyrus	0.045	0.036	0.015	0.025	0.034	NS	NS	NS	NS	NS	NS	NS	NS	NS	NS	NS	NS	NS	0.014	0.022	NS	NS	0.023	0.025	NS	NS	NS	0.049	NS	NS
3 - L	Post Central Gyrus	0.020	NS	0.030	0.019	0.036	0.014	0.045	NS	NS	NS	0.026	NS	NS	NS	NS	NS	0.035	NS	NS	NS	0.034	NS	NS	NS	0.050	NS	0.050	0.049	NS	0.050
3 - R	Post Central Gyrus	0.040	0.047	0.015	0.029	0.044	NS	NS	NS	NS	NS	NS	NS	NS	NS	NS	NS	NS	NS	0.018	0.030	0.029	NS	NS	0.042	0.039	NS	NS	NS	NS	NS
4 - L	Pre-Central Gyrus	0.021	NS	0.044	0.032	NS	0.026	NS	NS	NS	NS	0.029	NS	NS	NS	NS	NS	0.036	NS	NS	NS	0.044	NS	NS	NS	NS	NS	NS	NS	NS	NS
4 - R	Pre-Central Gyrus	NS	NS	0.016	0.038	NS	NS	NS	NS	NS	NS	NS	NS	NS	NS	NS	NS	NS	NS	0.016	0.033	0.030	NS	NS	NS	NS	NS	NS	NS	NS	NS
5 - L	Parietal Lobe	NS	NS	0.032	0.026	0.037	0.039	NS	0.011	0.019	NS	NS	NS	0.040	NS	NS	NS	0.025	0.020	0.022	0.030	NS	NS	NS	0.046	NS	NS	NS	NS	NS	NS
5 - R	Parietal Lobe	NS	NS	0.041	0.035	NS	NS	NS	0.021	0.031	NS	NS	NS	NS	NS	NS	NS	0.026	0.039	0.007	0.026	0.041	NS	NS	0.050	NS	NS	NS	NS	NS	NS
13a - L	Anterior Insula	0.007	NS	NS	NS	NS	NS	NS	NS	NS	NS	NS	NS	NS	NS	NS	NS	NS	NS	NS	NS	NS	NS	NS	NS	NS	NS	NS	NS	NS	NS
13a - R	Anterior Insula	0.015	NS	0.007	NS	NS	NS	NS	NS	NS	NS	NS	NS	NS	NS	NS	NS	NS	NS	NS	NS	NS	NS	NS	NS	NS	NS	NS	NS	NS	NS
24 - L	Anterior Cingulate Gyrus	0.013	NS	NS	0.044	NS	NS	NS	NS	NS	NS	NS	NS	NS	NS	NS	NS	NS	NS	NS	NS	NS	NS	NS	NS	NS	NS	NS	NS	NS	NS
24 - R	Anterior Cingulate Gyrus	0.015	NS	0.035	NS	NS	NS	NS	NS	NS	NS	NS	NS	NS	NS	NS	NS	NS	NS	NS	NS	NS	NS	NS	NS	NS	NS	NS	NS	NS	NS
32 - L	Anterior Cingulate Gyrus	0.015	NS	0.035	0.006	NS	NS	NS	NS	NS	NS	NS	NS	NS	NS	NS	NS	NS	NS	NS	NS	NS	NS	NS	NS	NS	NS	NS	NS	NS	NS
32 - R	Anterior Cingulate Gyrus	0.016	NS	0.005	0.010	NS	NS	NS	NS	NS	NS	NS	NS	NS	NS	NS	NS	NS	NS	NS	NS	NS	NS	NS	NS	NS	NS	NS	NS	NS	NS
33 - L	Anterior Cingulate	0.011	NS	NS	NS	NS	NS	NS	NS	NS	NS	NS	NS	NS	NS	NS	NS	NS	NS	NS	NS	NS	NS	NS	NS	NS	NS	NS	NS	NS	NS
33 - R	Anterior Cingulate	0.014	NS	NS	NS	NS	NS	NS	NS	NS	NS	NS	NS	NS	NS	NS	NS	NS	NS	NS	NS	NS	NS	NS	NS	NS	NS	NS	NS	NS	NS
Thal - L	Parasubiculum hippocampal region	0.049	NS	NS	NS	NS	NS	NS	NS	NS	NS	NS	NS	NS	NS	NS	NS	NS	NS	NS	NS	NS	NS	NS	NS	NS	NS	NS	NS	NS	NS
Thal - R	Parasubiculum hippocampal region	NS	NS	NS	NS	NS	NS	NS	NS	NS	NS	NS	NS	NS	NS	NS	NS	NS	NS	NS	NS	NS	NS	NS	NS	NS	NS	NS	NS	NS	NS
Hab - L	Habenula	NS	NS	NS	NS	NS	NS	NS	NS	NS	NS	NS	NS	NS	NS	NS	NS	NS	NS	NS	NS	NS	NS	NS	NS	NS	NS	NS	NS	NS	NS
Hab - R	Habenula	NS	NS	NS	NS	NS	NS	NS	NS	NS	NS	NS	NS	NS	NS	NS	NS	NS	NS	0.032	NS	NS	NS	NS	NS	0.010	NS	NS	NS	NS	NS
Amy - L	Amygdala	0.016	NS	NS	NS	NS	NS	NS	NS	NS	NS	NS	NS	NS	NS	NS	NS	NS	NS	NS	NS	NS	NS	NS	NS	NS	NS	NS	NS	NS	NS
Amy - R	Amygdala	0.040	NS	NS	NS	NS	NS	NS	NS	NS	NS	NS	NS	NS	NS	NS	NS	0.028	NS	NS	0.028	NS	NS	NS	0.049	0.044	NS	NS	NS	NS	NS

Supplement 3:

	Default Mode Network t-Test	Delta			Theta			Alpha			Beta																			
ROI-Name	ROI - LOCATION	1 Hz	2 Hz	3 Hz	4 Hz	5 Hz	6 Hz	7 Hz	8 Hz	9 Hz	10 Hz	11 Hz	12 Hz	13 Hz	14 Hz	15 Hz	16 Hz	17 Hz	18 Hz	19 Hz	20 Hz	21 Hz	22 Hz	23 Hz	24 Hz	25 Hz	26 Hz	27 Hz	28 Hz	29 Hz	30 Hz
2 - L	Post Central Gyrus	0.01 0	0.02 9	0.02 2	0.01 7	0.02 2	0.01 2	0.02 0	NS	NS	NS	NS	NS	NS	NS	NS	0.045	NS	0.035	NS	NS	0.029	0.044	NS	NS	NS	0.037	0.037	NS	0.044
2 - R	Post Central Gyrus	0.04 5	0.03 6	0.01 5	0.02 5	0.03 4	NS	NS	NS	NS	NS	NS	NS	NS	NS	NS	NS	NS	NS	0.014	0.022	0.024	NS	0.023	0.026	NS	NS	0.049	NS	NS
7 - L	Supramarginal Gyrus	0.02 3	0.04 0	0.01 1	0.02 0	0.01 0	0.01 0	0.03 3	0.01 3	NS	NS	0.050	NS	0.029	NS	NS	NS	NS	0.024	0.033	NS	0.038	NS	NS	0.039	NS	NS	NS	NS	NS
7 - R	Supramarginal Gyrus	NS	NS	0.02 6	0.02 8	0.04 2	NS	NS	NS	NS	NS	NS	0.045	NS	NS	NS	NS	0.050	0.022	NS	0.043	NS	NS	NS	0.031	NS	NS	NS	NS	NS
10 - L	Pre-Frontal Cortex	0.10 0	0.04 9	0.04 7	0.02 2	NS	NS	NS	NS	NS	NS	NS	NS	NS	NS	NS	NS	NS	NS	NS	NS	NS	NS	NS	NS	NS	NS	NS	NS	NS
10 - R	Pre-Frontal Cortex	0.01 6	0.04 3	0.01 1	0.04 2	NS	NS	NS	NS	NS	NS	NS	NS	NS	NS	NS	NS	NS	NS	NS	NS	NS	NS	NS	NS	NS	NS	NS	NS	NS
11 - L	Orbital Frontal	0.01 1	NS	0.00 7	NS	NS	NS	NS	NS	NS	NS	NS	NS	NS	NS	NS	NS	NS	NS	NS	NS	NS	NS	NS	NS	NS	NS	NS	NS	NS
11 - R	Orbital Frontal	0.01 2	NS	NS	NS	NS	NS	NS	NS	NS	NS	NS	NS	NS	NS	NS	NS	NS	NS	NS	NS	NS	NS	NS	NS	NS	NS	NS	NS	NS
19 - L	Occipital Cortex	NS	NS	0.03 7	0.03 1	NS	0.03 7	0.03 8	NS	NS	NS	NS	NS	NS	NS	NS	0.035	0.043	0.015	0.038	0.032	NS	0.037	NS	NS	NS	NS	0.049	NS	NS
19 - R	Occipital Cortex	NS	NS	0.04 0	0.04 7	0.04 4	NS	NS	NS	NS	NS	NS	NS	NS	NS	NS	0.035	NS	0.035	NS	NS	NS	NS	NS	NS	NS	NS	NS	NS	NS
29 - L	Posterior Cingulate & Superior Transverse Temporal Gyrus	NS	NS	NS	NS	NS	NS	NS	NS	NS	NS	NS	NS	NS	NS	NS	NS	NS	NS	NS	NS	NS	NS	NS	NS	NS	NS	NS	NS	NS
29 - R	Posterior Cingulate & Superior Transverse Temporal Gyrus	NS	NS	NS	NS	NS	NS	NS	NS	NS	NS	NS	NS	NS	NS	NS	NS	NS	NS	NS	0.018	0.014	0.046	0.035	0.003	0.023	NS	0.033	NS	NS
30 - L	Posterior Cingulate & Cuneus	NS	NS	NS	NS	NS	NS	NS	NS	NS	NS	NS	NS	NS	NS	NS	0.039	0.044	NS	0.048	NS	NS	0.042	NS	0.046	0.014	NS	0.033	NS	NS
30 - R	Posterior Cingulate & Cuneus	NS	NS	NS	NS	NS	NS	NS	NS	NS	NS	NS	NS	NS	NS	NS	NS	NS	NS	NS	NS	NS	0.022	NS	NS	NS	NS	NS	NS	NS
31 - L	Dorsal Posterior Cingulate	NS	NS	0.04 0	0.02 4	0.04 3	NS	NS	NS	NS	NS	NS	NS	NS	NS	NS	NS	0.031	NS	NS	NS	NS	NS	NS	NS	NS	NS	NS	NS	NS
31 - R	Dorsal Posterior Cingulate	NS	NS	0.04 8	0.03 8	NS	NS	NS	NS	NS	NS	NS	NS	NS	NS	NS	NS	NS	NS	NS	NS	NS	NS	NS	NS	NS	NS	NS	NS	NS
35 - L	Medial Temporal Lobe & Parahippocampal Gyrus	0.02 2	NS	NS	NS	NS	NS	NS	NS	NS	NS	NS	NS	NS	NS	NS	NS	NS	NS	NS	NS	NS	NS	NS	NS	NS	NS	NS	NS	NS
35 - R	Medial Temporal Lobe & Parahippocampal Gyrus	NS	NS	NS	NS	NS	NS	NS	NS	NS	NS	NS	NS	NS	NS	NS	NS	0.041	NS	0.047	0.016	NS	NS	NS	0.040	0.029	NS	NS	NS	NS	NS
39 - L	Angular Gyrus & Inferior Parietal Lobe	0.00 1	0.01 8	0.00 9	0.01 2	0.03 1	0.01 5	0.02 5	0.03 9	0.04 8	NS	NS	NS	0.038	NS	0.041	NS	0.020	0.032	0.023	0.036	0.017	NS	0.033	NS	0.044	0.038	NS	NS	NS
39 - R	Angular Gyrus & Inferior Parietal Lobe	NS	NS	0.03 1	0.03 1	0.04 0	0.04 7	NS	NS	NS	NS	NS	NS	NS	NS	NS	NS	0.050	0.019	0.038	0.019	NS	NS	0.029	0.017	NS	NS	NS	NS	0.044
40 - L	Inferior Parietal Lobe Angular Gyrus	0.00 5	0.02 2	0.01 6	0.01 1	0.02 5	0.01 2	0.01 9	0.04 1	NS	NS	0.042	NS	NS	NS	NS	0.039	NS	0.028	0.044	0.040	0.025	0.028	NS	0.047	NS	0.036	0.035	NS	0.044
40 - R	Inferior Parietal Lobe Angular Gyrus	NS	0.04 4	0.01 8	0.02 0	0.03 0	0.04 9	NS	NS	NS	NS	NS	NS	NS	NS	NS	NS	NS	NS	0.012	0.023	0.018	NS	NS	0.014	0.018	0.050	NS	0.045	NS	NS
Crus1 - L	Cerebellum	NS	NS	NS	NS	NS	NS	NS	NS	NS	NS	NS	NS	NS	NS	NS	0.011	0.031	NS	NS	NS	0.045	NS	0.035	NS	NS	NS	0.030	0.031	NS
Crus1 - R	Cerebellum	NS	NS	0.04 1	NS	NS	NS	NS	NS	NS	NS	NS	NS	NS	NS	NS	0.025	0.044	0.023	0.034	NS	NS	NS	NS	NS	NS	NS	0.041	NS	NS
Crus2 - L	Cerebellum	NS	NS	NS	NS	NS	NS	NS	NS	NS	NS	NS	NS	NS	NS	NS	0.017	0.035	NS	NS	NS	NS	NS	0.043	NS	NS	0.036	NS	0.030	0.029
Crus2 - R	Cerebellum	NS	NS	NS	NS	NS	NS	NS	NS	NS	NS	NS	NS	NS	NS	NS	0.019	0.040	0.023	0.042	NS	NS	NS	NS	NS	NS	NS	0.049	NS	NS
Cblm_9 - L	Cerebellum	NS	NS	NS	NS	NS	NS	NS	NS	NS	NS	NS	NS	NS	NS	NS	0.015	NS	NS	NS	NS	NS	NS	NS	NS	NS	NS	0.046	NS	NS
Cblm 9 - R	Cerebellum	NS	NS	NS	NS	NS	NS	NS	NS	NS	NS	NS	NS	NS	NS	NS	0.021	NS	0.049	0.049	NS	NS	0.043	NS	NS	NS	NS	0.042	NS	NS

Supplement 4

Pain Network		Talairach Coordinates		
Brodmann Area	ROI LOCATION	X	Y	Z
1 - L	Post Central Gyrus	−41	−40	67
1 - R	Post Central Gyrus	45	−37	63
2 - L	Post Central Gyrus	−44	−36	48
2 - R	Post Central Gyrus	46	−35	47
3 - L	Post Central Gyrus	−40	−28	51
3 - R	Post Central Gyrus	40	−28	51
4 - L	Pre-Central Gyrus	−31	−24	57
4 - R	Pre-Central Gyrus	31	−24	57
5 - L	Parietal Lobe	−11	−51	65
5 - R	Parietal Lobe	11	−51	66
13a - L	Anterior Insula	−34	18	−1
13a - R	Anterior Insula	36	18	−4
24 - L	Anterior Cingulate Gyrus	−4	17	29
24 - R	Anterior Cingulate Gyrus	5	16	30
32 - L	Anterior Cingulate Gyrus	−9	33	29
32 - R	Anterior Cingulate Gyrus	11	33	29
33 - L	Anterior Cingulate	−3	10	26
33 - R	Anterior Cingulate	4	11	26
Thal - L	Parasubiculum hippocampal region	−10	−20	8
Thal - R	Parasubiculum hippocampal region	10	−20	8
Hab - L	Habenula	−4	−28	−4
Hab - R	Habenula	4	−28	−4
Amy - L	Amygdala	−16	−4	−20
Amy - R	Amygdala	16	−4	−20

Supplement 5

Default Mode Network		Talairach Coordinates		
Brodmann Area	ROI LOCATION	X	Y	Z
2 - L	Post Central Gyrus	−44	−36	48
2 - R	Post Central Gyrus	46	−35	47
7 - L	Supramarginal Gyrus	−20	−66	51
7 - R	Supramarginal Gyrus	21	−66	52
10 - L	Pre-Frontal Cortex	−14	58	9
10 - R	Pre-Frontal Cortex	15	58	9
11 - L	Orbital Frontal	−15	41	−13
11 - R	Orbital Frontal	15	41	−13
19 - L	Occipital Cortex	−29	−75	6
19 - R	Occipital Cortex	30	−74	5
29 - L	Posterior Cingulate & Superior Transverse Temporal Gyrus	−9	−45	11
29 - R	Posterior Cingulate & Superior Transverse Temporal Gyrus	8	−44	11
30 - L	Posterior Cingulate & Cuneus	−15	−37	−13
30 - R	Posterior Cingulate & Cuneus	16	−37	−14
31 - L	Dorsal Posterior Cingulate	−5	−55	38
31 - R	Dorsal Posterior Cingulate	5	−55	38
35 - L	Medial Temporal Lobe & Parahippocampal Gyrus	−16	−13	−25
35 - R	Medial Temporal Lobe & Parahippocampal Gyrus	14	−13	−24
39 - L	Angular Gyrus & Inferior Parietal Lobe	−44	−64	28
39 - R	Angular Gyrus & Inferior Parietal Lobe	45	−64	29
40 - L	Inferior Parietal Lobe Angular Gyrus	−45	−46	43
40 - R	Inferior Parietal Lobe Angular Gyrus	46	−46	44
Crus1 - L	Cerebellum	−37	−66	−33
Crus1 - R	Cerebellum	38	−68	−33
Crus2 - L	Cerebellum	−29	−74	−39
Crus2 - R	Cerebellum	32	−70	−41
Cblm_9 - L	Cerebellum	−11	−50	−47
Clbm 9 - R	Cerebellum	9	−50	−47